Electronic Supplementary Information

Intercalation/deintercalation of solvated Mg^{2+} into/from graphite interlayers

Department of Materials Chemistry, Faculty of Engineering, Shinshu University
4-17-1 Wakasato, Nagano 380-8553, Japan

Masahiro Shimizu,* Atsuhito Nakahigashi, Susumu Arai

Dr. Masahiro Shimizu
Tel: +81-26-269-5627; Fax: +81-26-269-5432
E-mail: shimizu@shinshu-u.ac.jp

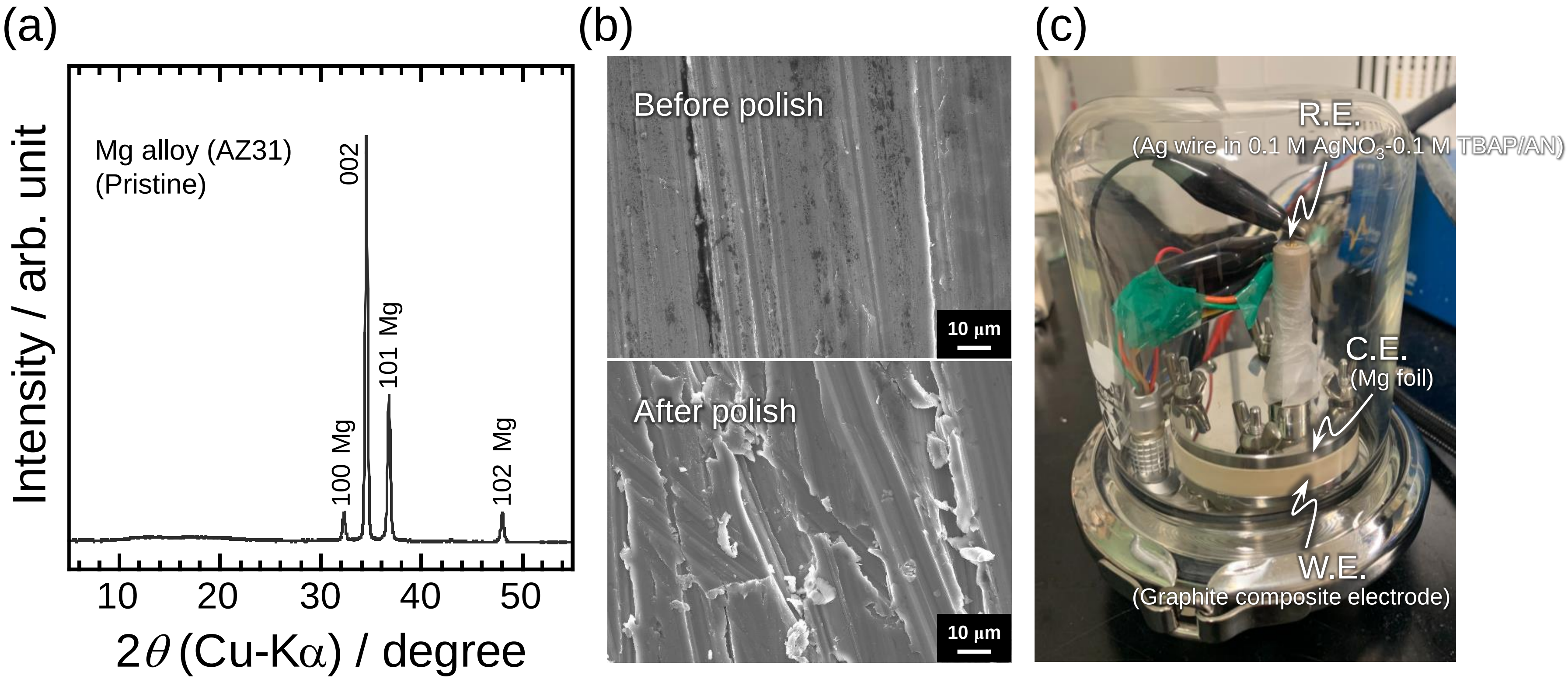

Figure S1. (a) XRD pattern of Mg alloy (AZ31) as the counter electrode. (b) SEM images of the Mg alloy before and after polish with a fine abrasive paper. (c) A three-electrode electrochemical cell used in this study. Before the assembly of the electrochemical cell, in order to progress Mg-stripping/deposition reactions smoothly on the counter electrode, we removed the surface passivation layers (oxidation layers) on the Mg alloy. Then, the change in the potential of the graphite electrode under a constant current density was recorded using the electrochemical cell sealed inside (c) an Ar-filled glass chamber.

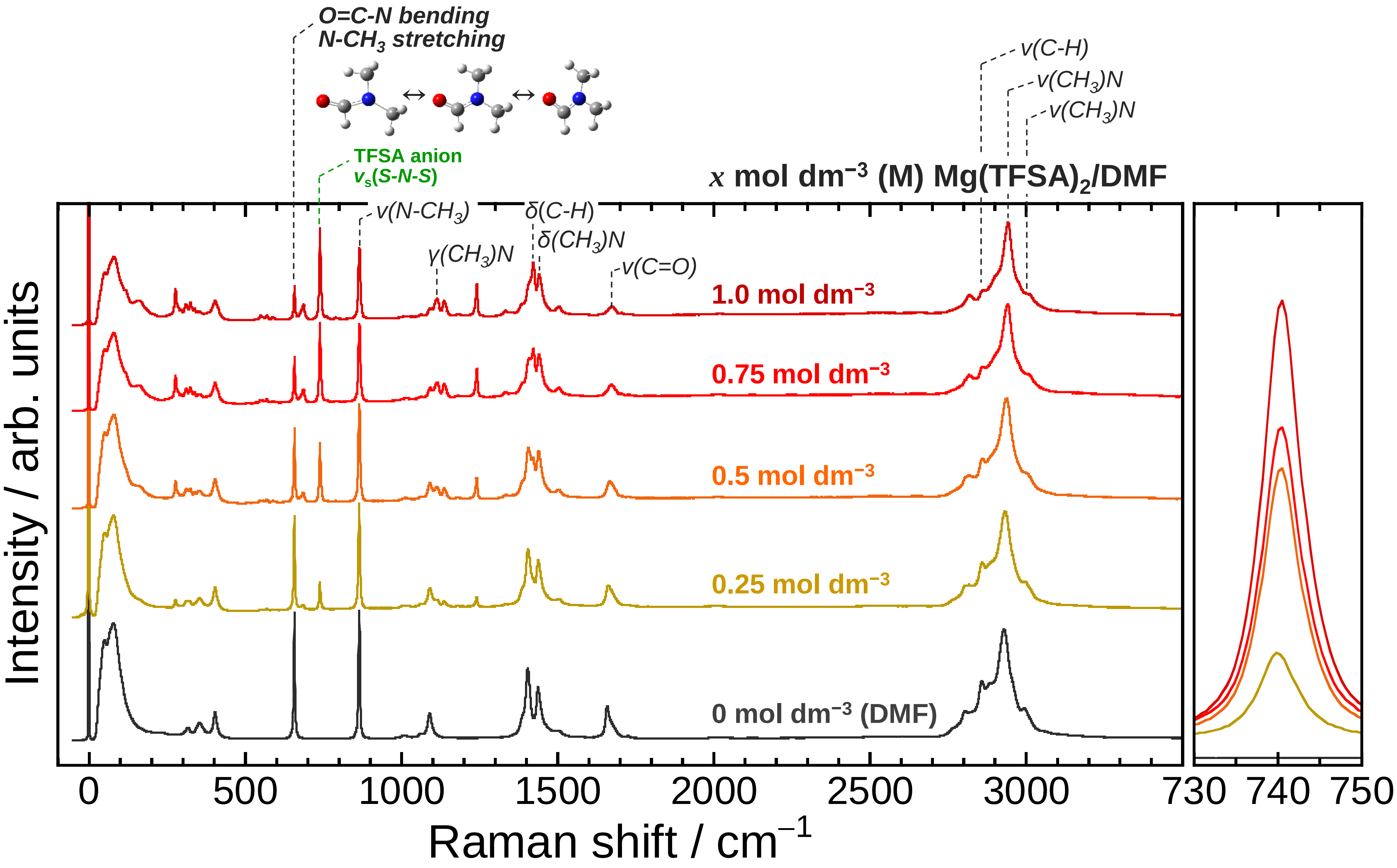

Figure S2. Raman spectra of electrolytes for *x* mol dm^{-3} (M) Mg(TFSA)$_2$/DMF in the frequency range of 0–3500 cm^{-1} (*x*=0, 0.25, 0.5, 0.75, 1.0).

Ref.) V. V. Chalapathi, K. V. Ramiah, *Proc. Natl. Acad. Sci. India A*, **68** (1968) 109–122.

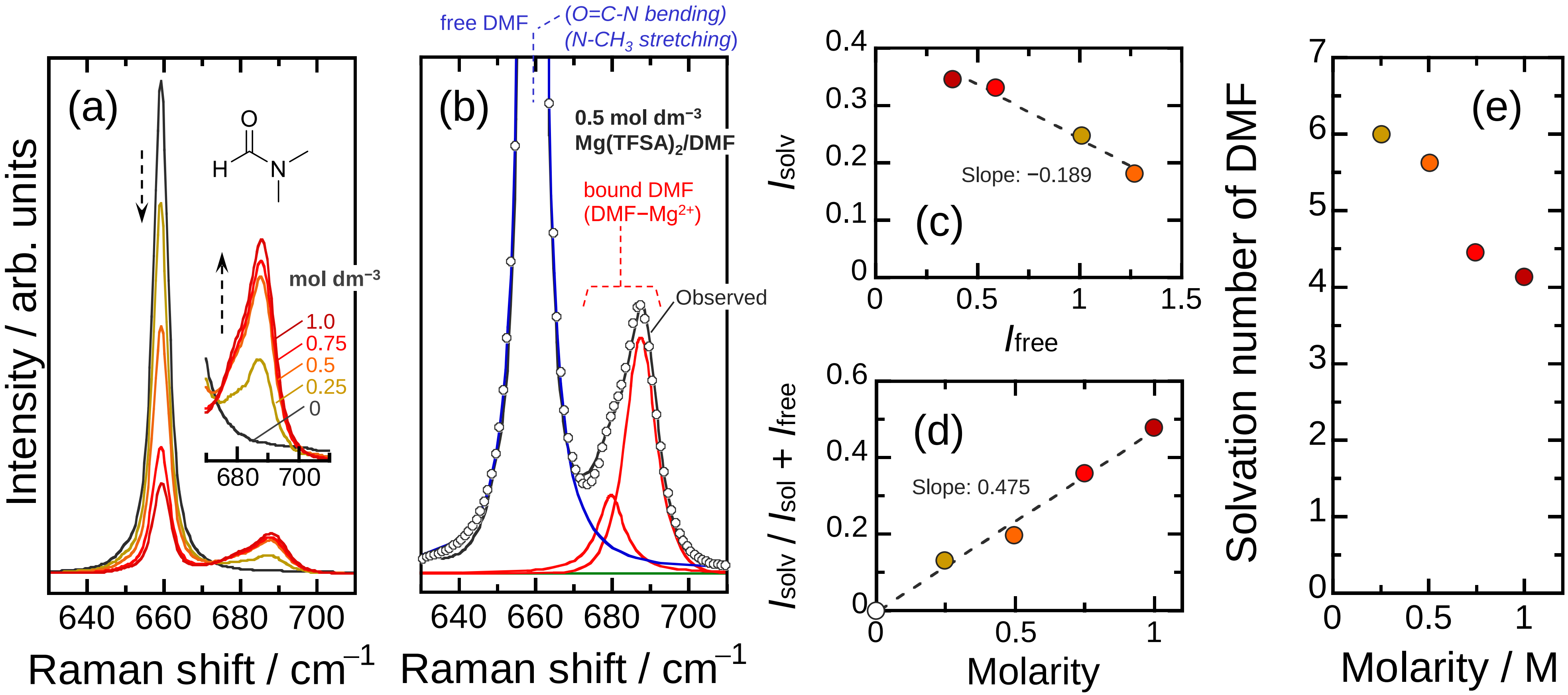

Figure S3. (a) Raman spectra of electrolytes for *x* mol dm^{-3} (M) Mg(TFSA)$_2$/DMF in the frequency range of 630−710 cm^{-1} (*x*=0, 0.25, 0.5, 0.75, 1.0). (b) Deconvoluted Raman bands of 0.5 M Mg(TFSA)$_2$/DMF: the black, blue, and red lines correspond to observed spectrum, free DMF, and bound DMF (interacting with Mg^{2+}). (c) Relation between intensities of free DMF (I_{free}) and DMF solvating Mg^{2+} (I_{solv}). (d) Plot of $I_{solv}/(I_{solv}+I_{free})$ versus Mg(TFSA)$_2$ molarity. (e) Average solvation number of DMF as a function of Mg(TFSA)$_2$ concentration.

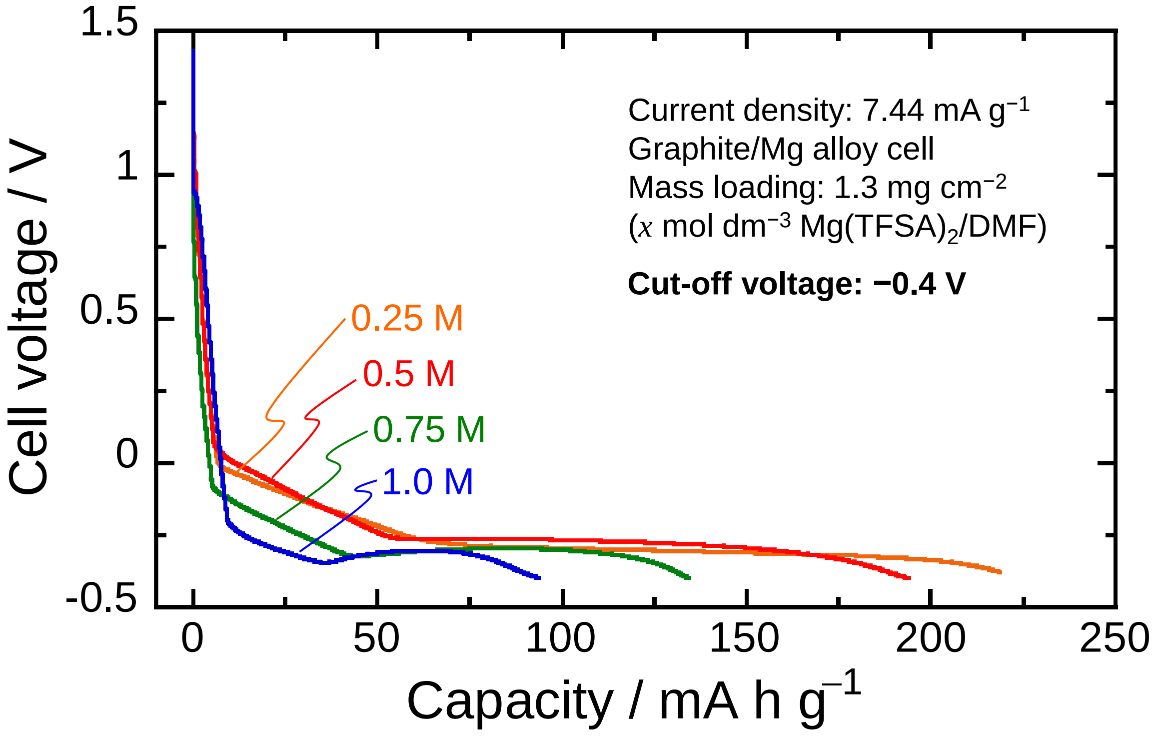

Figure S4. Galvanostatic charge curves of electrochemical cells with graphite/Mg alloy at current density of 7.44 mA g^{-1}. Each voltage plateau attributed to Mg^{2+} intercalation into graphite interlayer depended on salt concentrations: the plateau appeared at low voltage as with increasing in the concentration. Assuming that the potentials of the counter electrode (Mg alloy) did not undergo significant change during the charge process, 0.25 M and 0.5 M are suitable concentrations to enhance the intercalations of solvated Mg^{2+} into graphite interlayers.

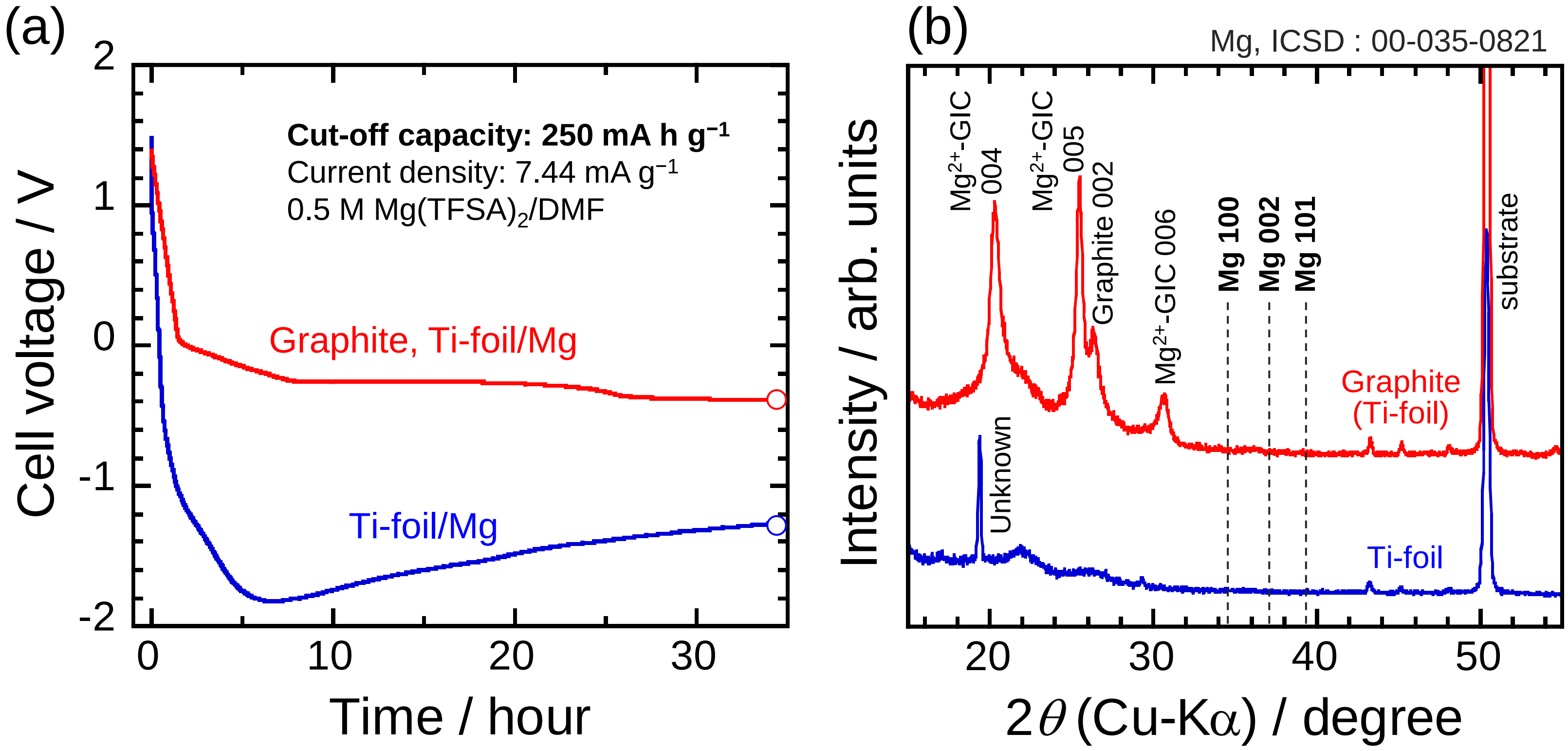

Figure S5. (a) Voltage changes in the graphite composite electrode with Ti foil (current collector) in a two-electrode type cell with Mg alloy (counter electrode). Current density: 7.44 mA g^{-1}, Electrolyte: 0.5 M Mg(TFSA)$_2$/DMF (b) XRD patterns of the graphite electrode and Ti foil after the DC polarization. In the XRD pattern after DC polarization, the electrodeposition of metallic Mg on the Ti foil was not detected, which suggested that Mg electrodeposition did not proceed in this electrolyte system even in the voltage of below 0 V.

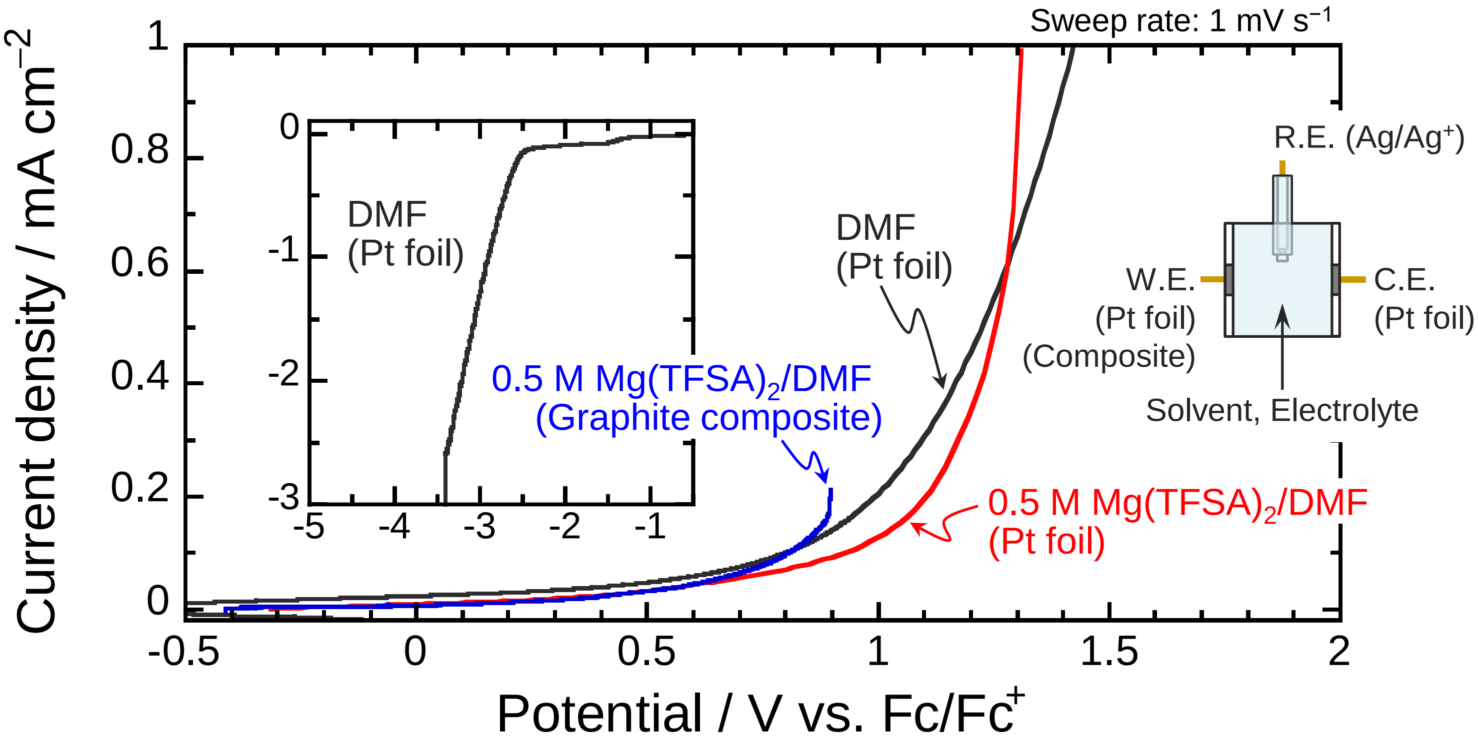

Figure S6. Linear sweep voltammograms of the DMF solvent with and without 0.5 M $Mg(TFSA)_2$ at sweep rate of 1 mV s^{-1} at room temperature (25 ^oC). Pt foils and a graphite composite which was used as a negative electrode were applied to the cathode in the voltammetry tests. With dissolution of $Mg(TFSA)_2$ into the DMF solvent, the oxidative decomposition of DMF slightly shifted to a higher potential side, which indicates that DMF is stabilized by the complex formation. Inset: linear sweep voltammogram of DMS solvent (with 20 mM tetrabutylammonium perchlorate: TBAP) during a cathodic scan. The potential of Ag/Ag^+ was converted to ferrocene/ferrocenium (Fc/Fc^+).

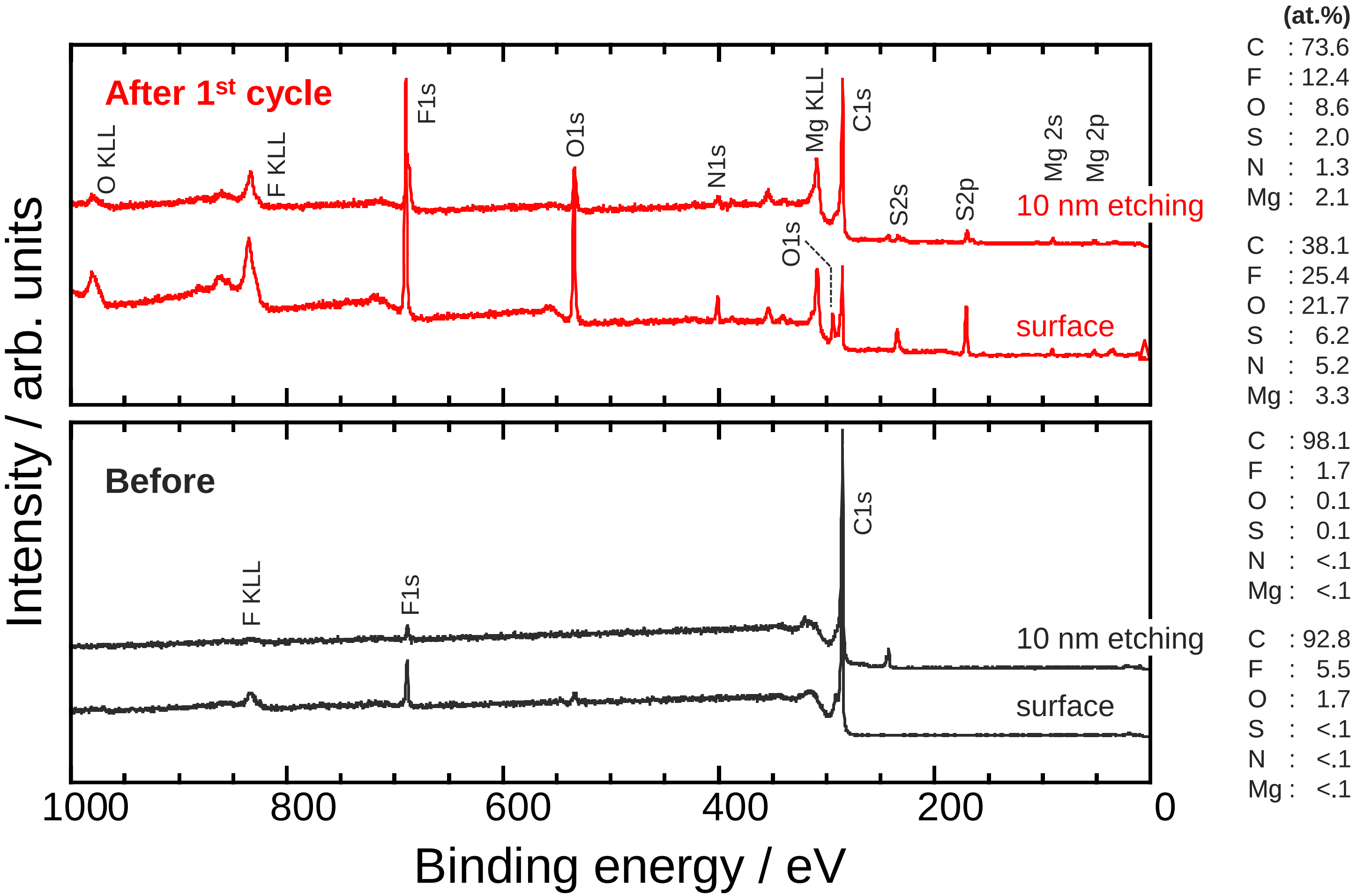

Figure S7. Survey XPS spectra of graphite composite electrodes before and after galvanostatic electrochemical tests. The incident X-ray source is monochromatic radiation (Al-Kα, 1486.6 eV) and was operated at 25 W (X-ray beam diameter: 100 μm, source analyzer angle: 45.0°). The sputtering was conducted at 2 kV, and the spectra were collected every 80 s.

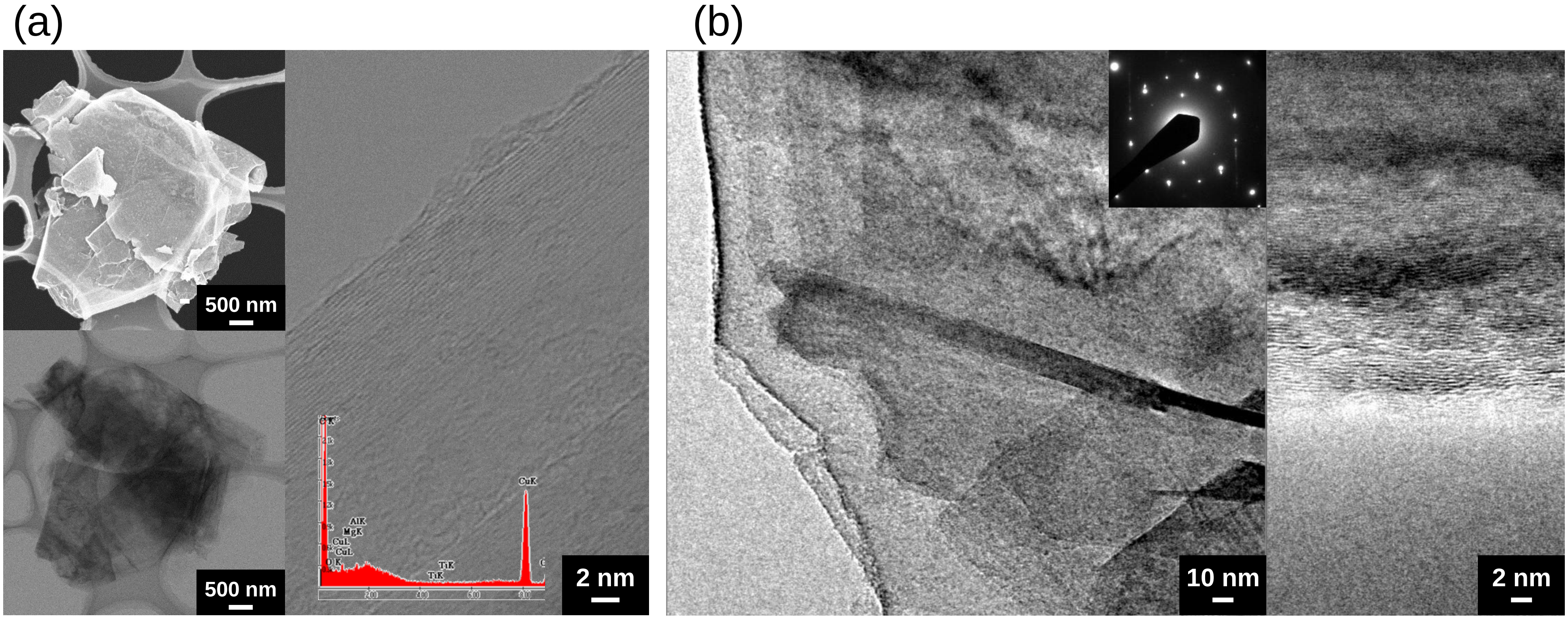

Figure S8. (a) STEM and (b) TEM images of graphite powder. Inset: selected area electron diffraction (SAED) patten. The graphite powder was removed from the composite electrode (10 wt.% PVDF binder) in the electrochemical cell after the first cycle (charge/discharge capacities: 250 mA h g^{-1}, current density: 7.44 mA g^{-1}, electrolyte: 0.5 M $Mg(TFSA)_2$/DMF). The graphite powder was dispersed into acetone and then held at a micro-grid structure for the TEM observation. Surface layers derived from the electrolyte decomposition seems to be formed at the edges of the graphite powder (right), and the thickness is ~4 nm.

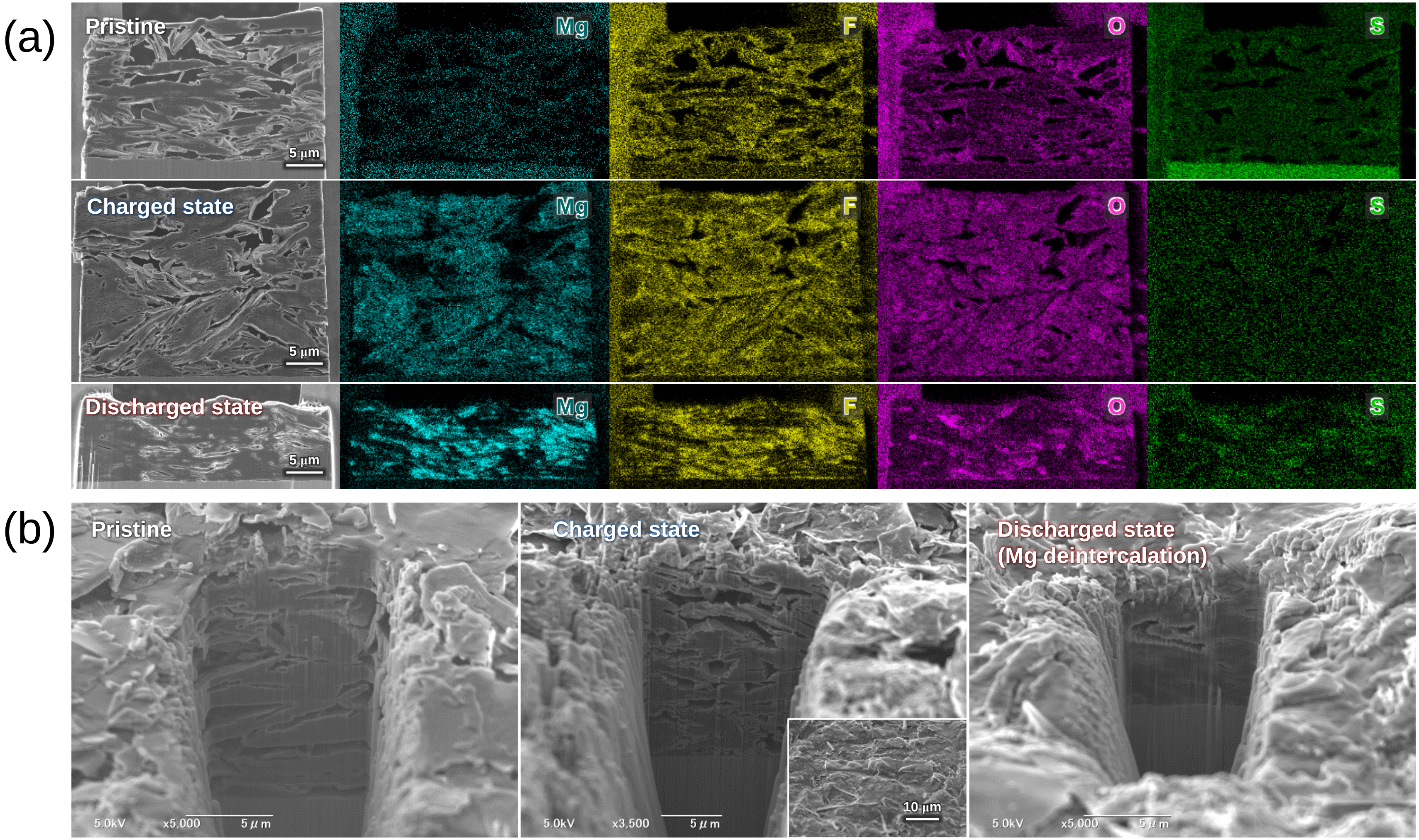

Figure S9. (a) Cross-sectional and (b) surface SEM images and EDS mapping of graphite composite electrodes before the electrochemical test and at charged and discharged states. After the first cycle with charge/discharge capacities of 250 mA h g^{-1}, the electrode resulted in compact and the thickness reversibly changed. Surface layers seem to be formed on graphite surface after the first cycle.

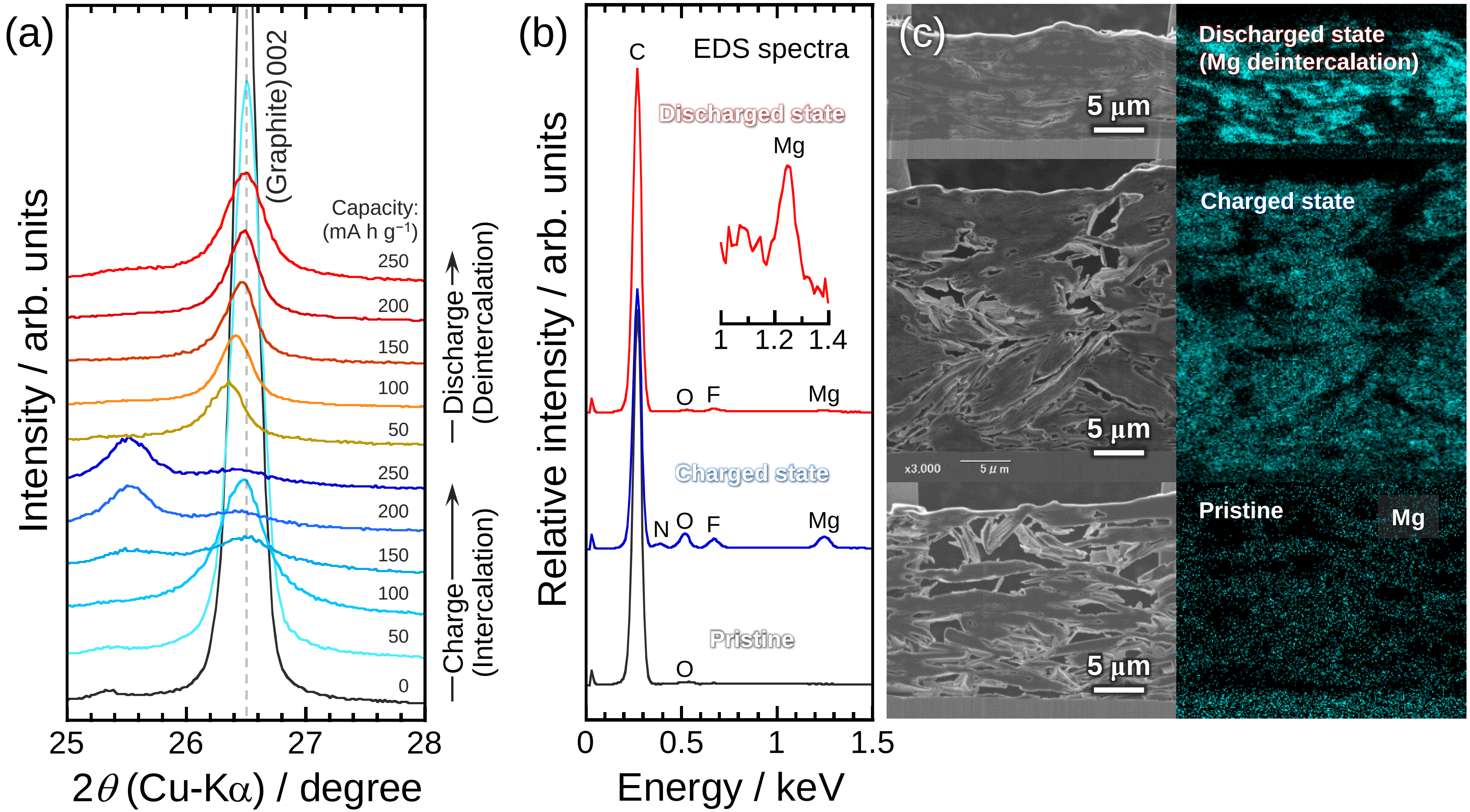

Figure S10. (a) Enlarged XRD patterns of the graphite electrodes (Figure 3) during the first galvanostatic charge–discharge cycle. (b) EDS spectra and (c) cross-sectional SEM images and EDS mapping images (Mg) of the graphite electrode before and after the first cycle. After the discharged state with a capacity of 250 mA h g^{-1}, the position of the 002 diffraction of the graphite completely returned to the original position as before charging.

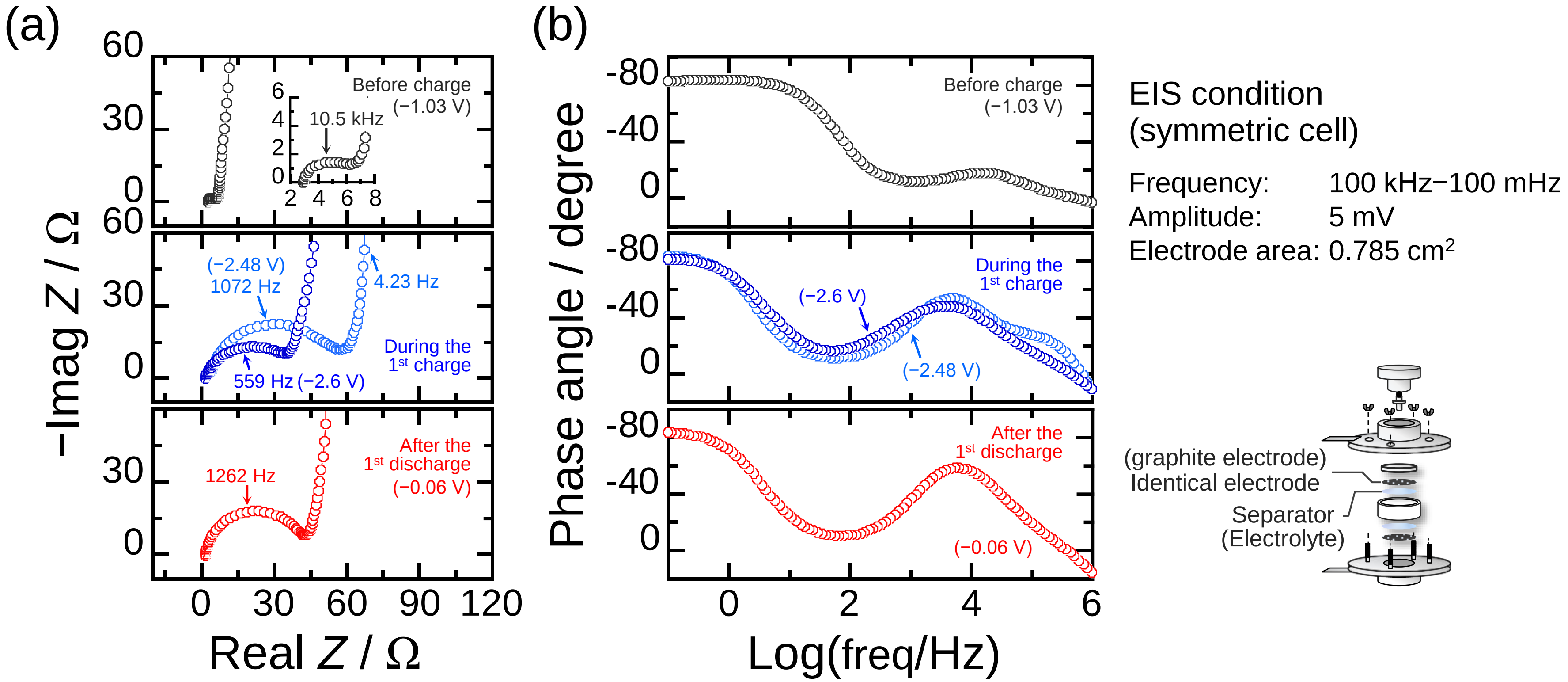

EIS condition
(symmetric cell)

Frequency: 100 kHz−100 mHz
Amplitude: 5 mV
Electrode area: 0.785 cm^2

Figure S11. (a) Nyquist plots and (b) Bode phase shift plots of symmetric cells consisting of graphite/graphite electrodes. The two identical graphite electrodes were prepared by the galvanostatic charge/discharge. The potential of Fc/Fc$^+$ was converted from the potential of Ag/Ag$^+$ (an Ag wire in 0.1 M AgNO$_3$-0.1 M TBAP/AN). Inset: a schematic diagram of the electrochemical-cell configuration for the impedance analysis. At the potential of −1.03 V vs. Fc/Fc$^+$ before the charging, one semicircle was detected at a high frequency region, which is assigned to the contact resistance between active materials, as typically observed in a Nyquist plot in electric double layer capacitors.